ISPRS Journal of Photogrammetry and Remote Sensing 166 (2020) 278–293

Contents lists available at ScienceDirect

ISPRS Journal of Photogrammetry and Remote Sensing

journal homepage: www.elsevier.com/locate/isprsjprs

Identifying floods and flood-affected paddy rice fields in Bangladesh based on Sentinel-1 imagery and Google Earth Engine

Mrinal Singha[a], Jinwei Dong[a,*], Sangeeta Sarmah[b], Nanshan You[a], Yan Zhou[a], Geli Zhang[c], Russell Doughty[d], Xiangming Xiao[d]

[a] Key Laboratory of Land Surface Pattern and Simulation, Institute of Geographic Sciences and Natural Resources Research, Chinese Academy of Sciences, Beijing 100101, China

[b] Key Laboratory of Ecosystem Network Observation and Modeling, Institute of Geographic Sciences and Natural Resources Research, Chinese Academy of Sciences, Beijing 100101, China

[c] College of Land Science and Technology, China Agricultural University, Beijing 100193, China

[d] Department of Microbiology and Plant Biology, University of Oklahoma, Norman, OK 73019, USA

ARTICLE INFO

Keywords:
Flood
Sentinel-1 SAR
Google Earth Engine
Bangladesh
Sentinel-2

ABSTRACT

Globally, flooding is the leading cause of natural disaster related deaths, especially in Bangladesh where approximately one third of national area gets flooded annually by overflowing rivers during the monsoon season, which drastically affects paddy rice agriculture and food security. However, existing studies on the pattern of floods and their impact on agriculture in Bangladesh are limited. Here we examined the spatiotemporal pattern of floods for the country during 2014–2018 using all the available Sentinel-1 Synthetic Aperture Radar (SAR) images and the Google Earth Engine (GEE) platform. We also identified the flood-affected paddy rice fields by integrating the flooding areas and remote sensing-based paddy rice planting areas. Our results indicate that flooding is frequent in northeastern Bangladesh and along the three major rivers, the Ganges, Brahmaputra, and Meghna. Between 2014 and 2018, the flood-affected paddy rice areas accounted for 1.61–18.17% of the total paddy rice area. The satellite-based detection of floods and flood-affected paddy rice fields advance our understanding of the annual dynamics of flooding in Bangladesh, which is essential for adaptation and mitigation strategies where severe annual floods threaten human lives, properties, and agricultural production.

1. Introduction

It is estimated that nearly one billion people live in flood-prone areas, and this number is predicted to double by 2050 due to erratic precipitation events and rapid population growth (UNU, 2018). Floods caused the loss of 6.8 million human lives in the 20th century globally, and a recent study showed that floods affected 2.3 billion people between 1995 and 2015 (Wahlstrom and Guha-Sapir, 2015), marking flood as the most deadly natural disaster (Doocy et al., 2013). In the context of climate change, the frequency and severity of flooding are increasing at an alarming rate, with a notable four-fold increase in Asia between 1982 and 2006 (Adikari and Yoshitani, 2009). Knowing the spatial extent and frequency of floods is an asset to government and disaster relief agencies and is necessary for delivering quick and efficient support to the people affected by floods. The catastrophic impacts of floods on the people and agriculture can be reduced with the identification of frequent flood-prone areas. Bangladesh is the fourth largest rice-producing country in the world (Bangladesh, 2019). However, food security is still a concern for this nation (Maclean et al., 2013), as local rice production is hampered by climate-induced natural hazards including flood, droughts, and cyclones. Among these disasters, flooding is the most common and substantially affects rice production in Bangladesh. Thus, the identification of frequently flooded areas and flood-affected rice paddies is essential for mitigating flood events, reducing property damage, and ensuring food security for Bangladesh.

Flooding is very common for low-lying Bangladesh (Islam et al., 2010). The country is comprised of flood plains along three major rivers: the Brahmaputra, Meghna, and Ganges. Flooding occurs along these three major rivers and their tributaries nearly every year during the monsoon season between June and September. Annually, almost one-third of Bangladesh is flooded by overflowing rivers induced by excess monsoon rains (Mirza, 2002). Bangladesh is densely populated,

* Corresponding author at: Institute of Geographic Sciences and Natural Resources Research, Chinese Academy of Sciences, 11A, Datun Road, Chaoyang District, Beijing 100101, China.

E-mail address: dongjw@igsnrr.ac.cn (J. Dong).

https://doi.org/10.1016/j.isprsjprs.2020.06.011
Received 11 January 2020; Received in revised form 28 May 2020; Accepted 16 June 2020

and floods affect a vast number of people. Periodic flooding plays a critical role in maintaining the flora and fauna along the rivers and lakes (Huang et al., 2014). Floods enhance the fertility of the soil to supply the necessary nutrients in the form of sediments carried in the flood water. If effectively stored, flood waters can also be used for long term water supply. However, floods severely damage property, buildings, roads, standing crops, and are deadly to livestock and humans. Thus, monitoring of flooding events is necessary. Disaster relief organizations are required to respond quickly, and near-real time flood maps are needed for relief operations. Additionally, maps of flood dynamics, frequency, and extent are essential for regional planning and policymaking for flood mitigation and adaptation and designing flood protection infrastructure.

The river gauge data and model simulations can predict the variation of flooded area at the country scale, but it is unable to provide the accurate spatial extent of flooded areas (Huang et al., 2014). Unlike the water level-based flood maps, the satellite-based flood maps provide the spatial distribution and extent of floods in various spatial resolutions over time and in near real time, and they can track frequently flooded regions with high efficiency and accuracy. Field-based surveys of flooded area are challenging and unfeasible for large areas, whereas satellite observation is a realistic choice for near-real time flood monitoring. Two types of satellite observations are available for monitoring flooded areas: optical imagery and Synthetic Aperture Radar (SAR) imagery. Data from a number of optical sensors, such as the Moderate Resolution Imaging Spectroradiometer (MODIS), Advanced Very High Resolution Radiometer (AVHRR), and Landsat, have been used to derive flood maps (Islam et al., 2010; Qi et al., 2009; Sheng et al., 2001). However, passive optical sensors are dependent on the solar reflectance and are unable to capture the earth surface during the cloudy days. The active sensor SAR is capable of collecting data through the cloud cover and is suitable for flood monitoring (Clement et al., 2018; Long et al., 2014; Matgen et al., 2011), and is especially advantageous in areas with persistent cloud cover and a rainy monsoon season. Flooded areas generate a low backscatter signal, and water surfaces appear to be very dark in SAR images, which makes them distinguishable from the other land cover classes like vegetation, agricultural land, bare land, or built-up areas. Some challenges remain when using SAR for flood detection (Notti et al., 2018). For instance, the temporary roughness of water surface, caused by the wind or heavy rainfall during the key flooding period, may complicate the detection of some flooded areas (Brisco et al., 2009); the radar shadow present in the SAR images are dark and can be misclassified as a flood water (Mason et al., 2010); and the double-bounce backscatter signal and radar shadows produced from high densities of buildings in urban areas hampers the correct identification of flooded areas. Nevertheless, the ability of SAR to collect data through dense cloud clover during the rainy season and the abundant availability of Sentinel-1 data makes SAR a key tool in flood mapping and monitoring.

Several SAR-based flood detection techniques have been proposed (Tsyganskaya et al., 2018), which primarily uses a single method or with the combination of multiple methods. These include histogram thresholding or clustering (Martinis et al., 2009), fuzzy classification (Martinis et al., 2018; Twele et al., 2016), region growing (Martinis et al., 2015; Mason et al., 2012), and texture analysis (Ouled Sghaier et al., 2018; Pradhan et al., 2014; Senthilnath et al., 2013). Most of these techniques use an image from a single date to detect flooding events. The multi-temporal change detection methods use a time series of images to detect the differences in pre-flood and post-flood land cover (Li et al., 2018; Long et al., 2014). The land cover difference image is combined with other techniques such as histogram thresholding or image segmentation to identify flooded areas (Clement et al., 2018). This method yields higher accuracy compared to a single image-based method. Some methods use high resolution elevation maps to detect floods (Manfreda et al., 2011; Sanders, 2007). However, elevation-based maps are not effective in the low-lying regions such as Bangladesh. Previously, a combination of optical image (Landsat 8) and SAR (COSMO-SkyMed) images were used to map floods using support vector machine classifiers in China (Tong et al., 2018). In an amalgamated method, the combination of texture analysis with the fuzzy classification system and the change detection approach was used to map floods using Sentinel-1 SAR data (Amitrano et al., 2018). Recently, the probability based approach was developed to map floods using the SAR images (Hostache et al., 2018). Crowd sourced data has also been combined with satellite data and geo-statistical analysis were also used to derive flood extent maps (Panteras and Cervone, 2018).

For Bangladesh, Islam et al. (2010) identified flooded areas using MODIS images for 2004 and 2007. Hoque et al. (2011) used RADARSAT data from 2000 to 2004 for flood mapping in the Maghna River basin of Bangladesh. However, flood patterns in Bangladesh never have been analyzed with a time series of SAR images at a high spatial and temporal resolution. The flood-affected paddy rice planting area is also unknown in Bangladesh. In our study, to increase the flood identification accuracy, we used two methods: the Change Detection and Thresholding (CDAT) (Long et al., 2014) and Normalized Difference Flood Index (NDFI)-based approaches (Cian et al., 2018). These two methods have proven to be reliable in mapping floods accurately using time series SAR data. However, SAR-based flood mapping has been limited to small study areas due to the intensive amount of data processing. With the recent development of high performance cloud computing platforms like Google Earth Engine (GEE) (Gorelick et al., 2017), NASA Earth Exchange (Nemani et al., 2011), Amazon Web Services (Jackson et al., 2010), computationally expensive geospatial data analysis has become possible. However, the use of these cloud computing techniques in remote sensing applications is still in its infancy. In this study, we used GEE to map flooded areas in near-real time for a very large area and analyzed a huge volume of SAR time series data.

Our objective was to map flooded areas, analyze their frequency, and determine the flood-affected paddy rice planting areas using Sentinel-1 SAR data, the GEE cloud computing platform, and paddy rice maps from our previous study (Singha et al., 2019). We would like to answer the following research questions: (1) what are the annual spatial patterns and dynamics of floods in Bangladesh from 2014 to 2018; and (2) how were the paddy rice fields affected by flooding in Bangladesh? This study will advance our knowledge on flooding in Bangladesh by: (1) mapping floods at large-scales in near-real time and tracking its spatial–temporal dynamics at high spatial resolution; and (2) determining the paddy rice planting areas that are frequently affected by floods. Bangladesh is very vulnerable to flood-induced disasters due to its geography, climate, topography, and numerous rivers. The spatio-temporal and immediate knowledge of flooding is necessary to effectively reduce its destructive impact on croplands, ecosystems, property, social welfare and human health. To our knowledge, our study is the first to illustrate the spatiotemporal dynamics of flood events for densely populated Bangladesh and the paddy rice fields. We expect our maps to aid in flood management, disaster planning and response, food security, policy making, and water resource utilization.

2. Materials and methods

2.1. Study area

Bangladesh is situated in South Asia (Fig. 1) and is one of the most flood-prone countries in the world. It covers a land mass of approximately 147,000 km^2 and extends from 20°44′00″ to 26°37′51″N latitude and 88°0′14″ to 92°40′08″E longitude. The total population of Bangladesh is about 163 million. The topography of Bangladesh is primarily flat except for the Chittagong Hill Tracts (CHT) regions in the southeast with an average elevation over 300 m. The Ganges, Brahmaputra, and Meghna are the three main rivers and 230 smaller rivers flow across Bangladesh. The country has a subtropical monsoon climate with an annual average temperature ranging from 18 °C to 29 °C. The average

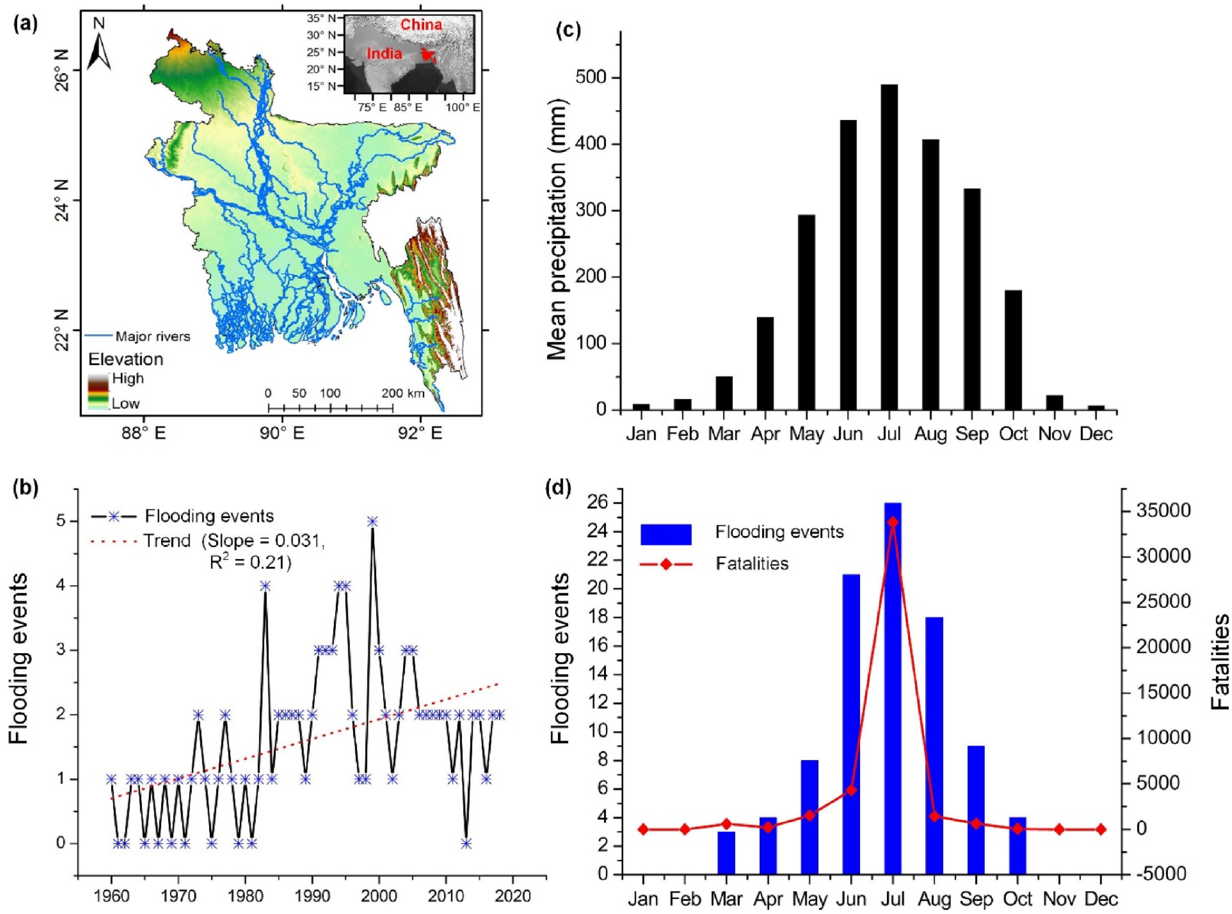

Fig. 1. Brief introduction of the study area. (a) Location of the study area including the elevation and major rivers; (b) annual total number of flood events and their trends (source of data: EM-DAT, The International Disaster Database); (c) mean monthly rainfall during 1981–2018, calculated from the Climate Hazards Group InfraRed Precipitation with Station Data (CHIRPS) (Funk et al., 2015); (d) total number of flood events and fatalities between 1960 and 2018 in Bangladesh (source of data: EM-DAT, The International Disaster Database).

annual precipitation ranges between 200 mm and 2000 mm, and about 80% of precipitation occurs during the monsoon season between June and September. The intensity, magnitude, and duration of precipitation in the three river basins (Ganges, Brahmaputra, and Meghna Basins) is a major determinant of flooding in Bangladesh. Agriculture areas cover around 70% of the country and paddy rice is the major crop with some areas being harvested up to three times per year. Severe flooding usually destroys paddy rice crops in Bangladesh.

Continuous rainfall caused flooding in Bangladesh in recent years (Fig. 1). The EM-DAT database showed an uneven temporal distribution of 94 flood events between 1960 and 2018, but generally there has been an increasing trend in flood frequency. Floods were most prevalent between May and October, co-occurring with the high monsoon rains (Fig. 1c). It was reported that a total of 52,616 people died due to floods between 1960 and 2018, which mostly occurred between May to October (Fig. 1b, d). Apart from taking lives, floods have damaged an innumerable number of houses, infrastructure, and crops in Bangladesh. It is expected that flooding events will increase in the coming decades as the climate changes.

2.2. Data

2.2.1. Sentinel-1 SAR data and processing

The Sentinel-1 Synthetic Aperture Radar (SAR) C-band (5.4 GHz) data is provided by the European Space Agency (ESA) and is freely available to the public (Torres et al., 2012). This global dataset has a 12 day or 6 day revisit cycle depending on the availability of Sentinel-1B imagery (Malenovský et al., 2012). Sentinel-1 satellite collects SAR imagery in four modes: Stripmap (SM), Interferometric Wide Swath (IW), Extra Wide Swath (EW), and Wave (WV) with various resolutions, polarizations, and extents for a variety of purposes. For our study, we used the IW mode, which meets the most current service requirements, avoids conflicts, and preserves revisit performance. The IW mode also provides consistent long-term archives and is particularly designed to acquire imagery of land surfaces (Torres et al., 2012). The IW-mode SAR imagery is provided in dual-polarization with vertical transmit and vertical receive (VV), and vertical transmit and horizontal receive (VH). The spatial resolution of this imagery is 10 m. We used the Level-1 Ground Range Detected (GRD) product, processed to the backscatter coefficient (σ^0) (Sentinel-1 Algorithms, 2019). The GRD scenes constitute of focused SAR data that has been detected, multi-looked, and projected to the Earth ellipsoid model WGS84 (Sentinel-1 Algorithms, 2019).

The Google Earth Engine pre-processed the Sentinel-1 data to derive the backscatter coefficient in each pixel using the following steps: (1) apply orbit file (to update orbit metadata with a restituted orbit file); (2) GRD border noise removal (removes low intensity noise and invalid data on scene edges); (3) thermal noise removal (removes additive noise by reducing discontinuities in sub-swaths for multi-swath acquisition); (4) radiometric calibration (calibrate backscatter intensity using sensor calibration parameters); (5) terrain corrections using SRTM or ASTER DEM (converts the data from ground range geometry to backscatter coefficient (σ^0) to account for terrain characteristics); and (6) the data were converted to decibels via log scaling (10*log10(x)) and

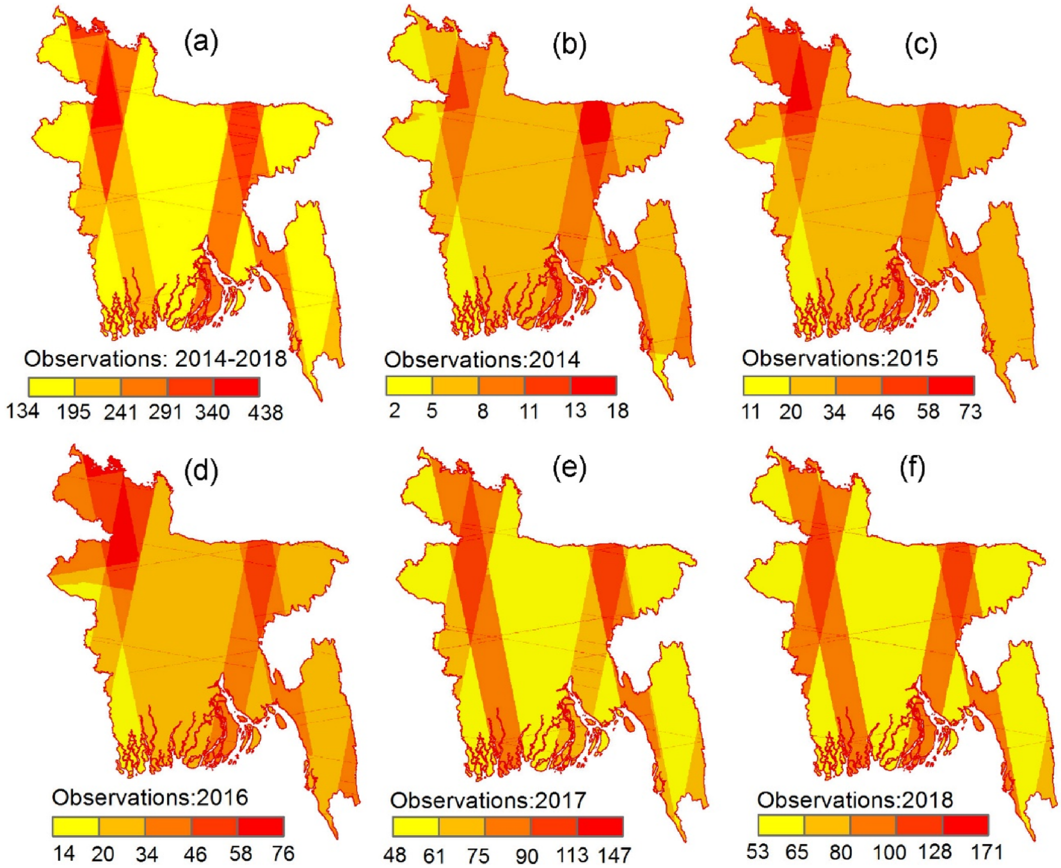

Fig. 2. Availability of time series Sentinel-1 images during the study period. (a) the total observation numbers between 2014 and 2018; (b) total number of observations in 2014; (c) total number of observations in 2015; (d) total number of observations in 2016; (e) total number of observations in 2017; (f) total number of observations in 2018.

quantized to 16-bits. We used all the available Sentinel-1 SAR datasets (2148 scenes) of Bangladesh for 2014–2018. The VV polarized data were selected from Sentinel-1 for flood mapping for its accuracy in detecting floods (Clement et al., 2018). Total number of observations of available Sentinel-1 images were shown in Fig. 2.

2.2.2. *Paddy rice maps of Bangladesh*

The paddy rice maps of Bangladesh for the year of 2017 were obtained from Singha et al. (2019). The maps were developed using the Sentinel-1 SAR datasets. The dataset is available for three rice cropping seasons in Bangladesh (Supplementary Fig. 1). The maps were produced at 10-m resolution using the Random Forest classifier, time series Sentinel-1 satellite data, and the Google Earth Engine. The maps were validated using samples generated from multiple sources, including ground truth samples and visual interpretation of very high spatial resolution images and Sentinel-2 images. The maps were also compared with the MODIS-based maps. The provided paddy rice maps had a satisfactory overall accuracy above 90%. Flood affected paddy rice planting areas were identified based on these maps assuming there were no drastic changes of paddy rice planting areas during the study period of 2014–2018.

2.2.3. *Other data*

(1) Sentinel-2 MSI. Sentinel-2 images were used to generate optical based flood map to evaluate the spatial pattern of the SAR based flood map. Sentinel-2 MSI (multispectral Instrument) images are provided by European Space Agency (ESA). This dataset contains 13 spectral bands including three QA bands, and the spatial resolution ranges from 10 m to 60 m depending on the bands. The revisit interval of the Sentinel-2 satellite is 5 days. We used NIR (band 8), red (band 4), and green (band 3) spectral bands with 10 m spatial resolution Top-Of-Atmosphere (TOA) Level 1C product. All the available images for Bangladesh during 2018 was used for the analysis and we selected the least cloudy pixels to generate the composites. These images were accessed using the Google Earth Engine (GEE).
(2) Earth's surface water dataset from 1984 to 2015 (https://global-surface-water.appspot.com/). This high resolution dataset was generated using Landsat satellite imagery at a global scale (Pekel et al., 2016). This dataset shows the changes in Earth's surface water over the past 32 years. This dataset was used to derive long term flood frequency to check the similarities of the Sentinel-1 based flood frequency.
(3) DEM data. We also used the 30 m resolution elevation data from the Shuttle Radar Topography Mission (SRTM) to mask hilly terrain, which is unlikely to flood.
(4) The flood archive data were derived from the International Disaster Database (EM-DAT) (https://www.emdat.be/). This dataset contains the flooding location, flood area, and total fatalities from 1960 to 2018.
(5) We also used flood archive data from the Darthmouth Flood Observatory (DFO). This dataset contains information on large floods from 1985 to 2018, including flood location, total flooded area, and cause. All the datasets we used are summarized in Table 1.

2.3. *Methods*

The methodology of this study includes the following key components: (1) flooded area identification using the Sentinel-1 SAR data by

Table 1
A summary of the datasets used for this study.

Data	Period	Resolution	Provided by	Source	Purpose in this study
Sentinel-1 satellite data	2014–2018	10 m	European Space Agency (ESA)	Google Earth Engine	To extract flooded areas and input for the model of flood-prone paddy rice area identification
Sentinel-2 satellite data	2017	10 m	European Space Agency (ESA)	Google Earth Engine	To extract flooded areas
Global Surface Water Layers	1984–2015	30 m	Pekel et al. (Pekel et al., 2016)	Google Earth Engine	To calculate long term flood frequency
Paddy rice maps	2017	10 m	Singha et al. (Singha et al., 2019)	https://doi.org/10.6084/m9.figshare.7873157.v1	To estimate paddy rice areas affected by floods
SRTM DEM	2000	30 m	NASA Jet Propulsion Laboratory (JPL)	Google Earth Engine	To mask the hilly terrains
EM-DAT Flood Archive	1960–2018	–	Centre for Research on the Epidemiology of Disasters (CRED)	https://www.emdat.be/	To validate the flood maps generated from Sentinel-1
DFO Flood Archive	1985–2018	–	Dartmouth Flood Observatory	https://www.dartmouth.edu/~floods/index.html	To validate the flood maps generated from Sentinel-1

integrating the Change Detection and Thresholding (CDAT) algorithm and the Normalized Difference Flood Index (NDFI); (2) determination of flood frequency of extreme flood events during the study period; (3) flood-affected paddy rice planting area identification using the derived flood extent maps. A flowchart of the methodology is shown in the Fig. 3. The Sentinel-1 SAR time series dataset was used to extract the flooded areas in Bangladesh for 2014–2018. The Sentinel-2-based flood extent map was used to validate and compare the Sentinel-1 SAR-based flood maps. The Landsat surface water datasets were used to derive the long-term flood frequency map, it also served for the verification of Sentinel-1 based flood frequency map.

2.3.1. Flood extent mapping by combining the CDAT and NDFI algorithms

(1) **The Change Detection and Thresholding (CDAT) algorithm.** The CDAT algorithm (Long et al., 2014) was adopted to identify the flooded area. The following steps were applied: (1) generate an absolute difference image (D) using a reference image (R) and a flooded image (F); and (2) classify the difference image (D) using thresholds to extract the flooded region. The reference image (R) in this study was calculated as a median value composite using the images from December and January (Clement et al., 2018), which are the driest months of the year and had no recorded floods in the study period. In the difference image (D), the flooded area in the image appeared to be darker, while the areas that appeared gray in both images indicated no changes. The flooded area creates a large negative difference due to the low backscatter radar signals from the water, compared to the high backscatter from the non-water areas. In the second step, a threshold is applied to identify the pixels that are flooded. The threshold was determined by the following criteria:

$$F_p < (\{\mu[D]\} - k_c * \{\sigma[D]\}) \tag{1}$$

where F_p are the flooded pixels, μ and σ are the mean and standard deviation of the difference image (D) respectively. k_c is a coefficient and the optimum value is 1.5 (Clement et al., 2018; Long et al., 2014).

(2) **The Normalized Difference Flood Index (NDFI) algorithm.** Flooded areas were also extracted using the NDFI algorithm (Cian et al., 2018). The NDFI is based on multi-temporal analysis of Sentinel-1 datasets. The NDFI was calculated as shown below in Eq. (2), where σ_0 is the backscatter of each pixel.

$$NDFI = \frac{mean\sigma_0(reference) - min\sigma_0(reference + flood)}{mean\sigma_0(reference) + min\sigma_0(reference + flood)} \tag{2}$$

The NDFI highlights the flooded areas considering the normal condition of earth surfaces and the temporarily covered water areas. The mean backscatter value in the multi-temporal reference image stack represents the average or normal characteristics of the land surface that include the low values from the smooth surfaces and the high values from the rough surfaces. The minimum value in the combined reference and flood stack capture the very low backscatter values generated due to flood. The difference between the mean and minimum value highlight the low backscatter values, i.e. flooded areas. In NDFI, the non-flooded areas have the values close to zero and can easily be masked out. The NDFI has several advantages. First, robustness and simplicity, NDFI requires minimum user dependent input and works in various environments with various sensors data (Cian et al., 2018). Second, it allows for an easy selection of threshold values due to the normalized index. Third, it can be utilized on large volumes of data.

(3) **Flood extent mapping by combining the CDAT and NDFI algorithms.** A "consistency map" (Arnell and Gosling, 2016) or a common map of flood extent was constructed that showed flooding areas common for both the CDAT and NDFI algorithms. The consistency map was considered as the actual flooding and used in the

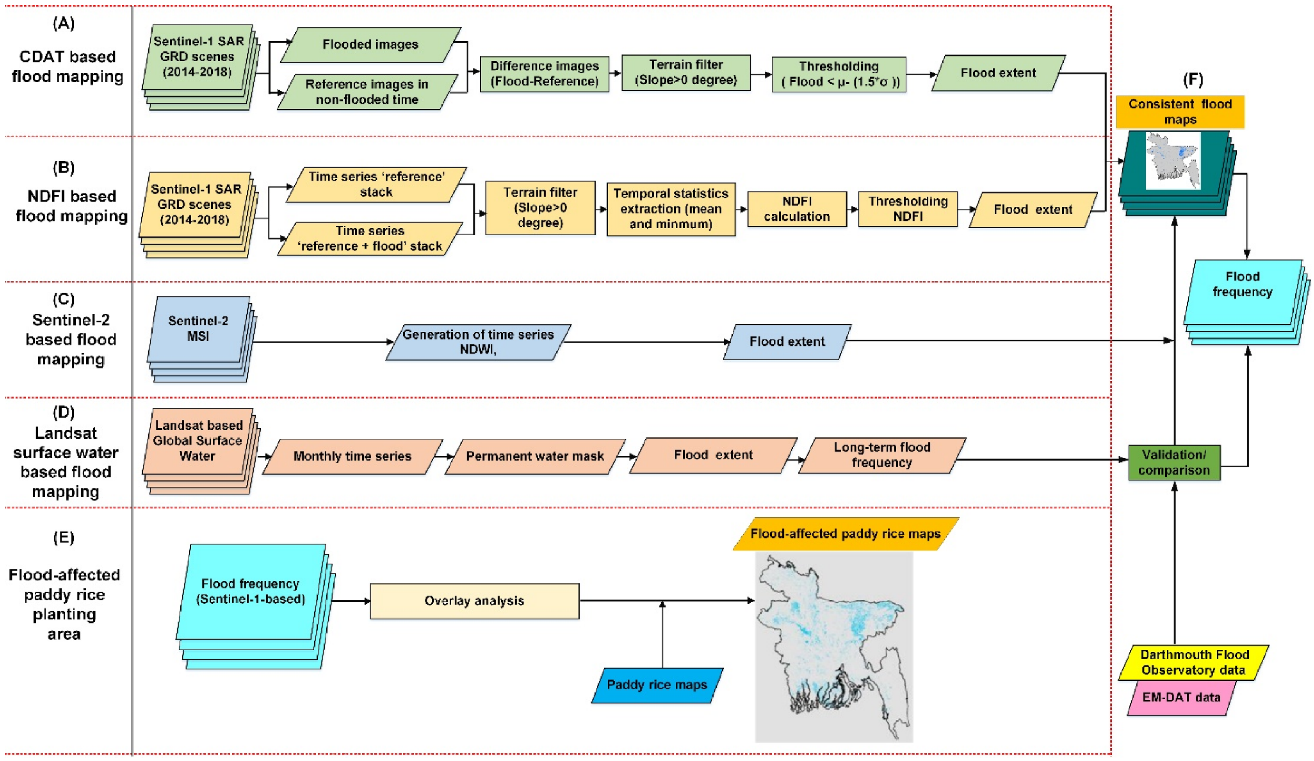

Fig. 3. Flowchart of the methodology comprised of five parts (A-E).

further analysis. The flooded areas for each year were added to obtain an image showing how many times a specific pixel was inundated within that year. This sum enables us to know the frequency and duration of floods for a certain year. For each individual year from 2014 to 2018, a time series of flood maps were created, which is the longest SAR-based high-resolution flood maps for Bangladesh.

2.3.2. Selection of most adequate reference image for CDAT and NDFI flood extent mapping

SAR-based flood mapping algorithms are often based on change detection techniques like CDAT and NDFI, which compares the backscattering signals between a reference image and a flooded image (Fig. 4a, b). The reference image represents an area under 'normal conditions', which helps to determine the changes in the SAR backscatter coefficient during flooding conditions. The flood maps produced from the change detection technique greatly depend on the selected reference image. The most adequate reference images need to be selected to minimize any under or over detection of flood. Hostache et al. (2018) suggested that reference image should be from the driest month that best represent the non-flood conditions. In our study, the reference image was calculated as a median value composite using the images from the month of December, January, and February (Fig. 4a). A case study conducted by Hostache et al. (2018) in Bangladesh also found the reference image from these months to be appropriate. These three months provide the highest number of SAR images during the driest time in the study region and are the preferred reference image for accurate flood mapping. We cross-referenced the DFO and EM–DAT flood archive to ensure that no flood events occurred during these time periods to avoid the inclusion of any images that may have captured

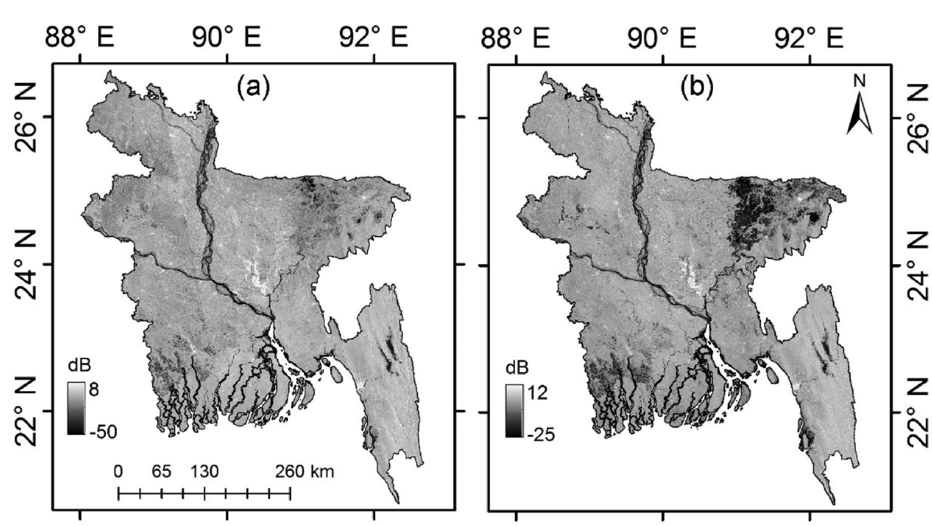

Fig. 4. Sentinel-1 composites from 2018. (a) Reference image; (b) flooded image in June.

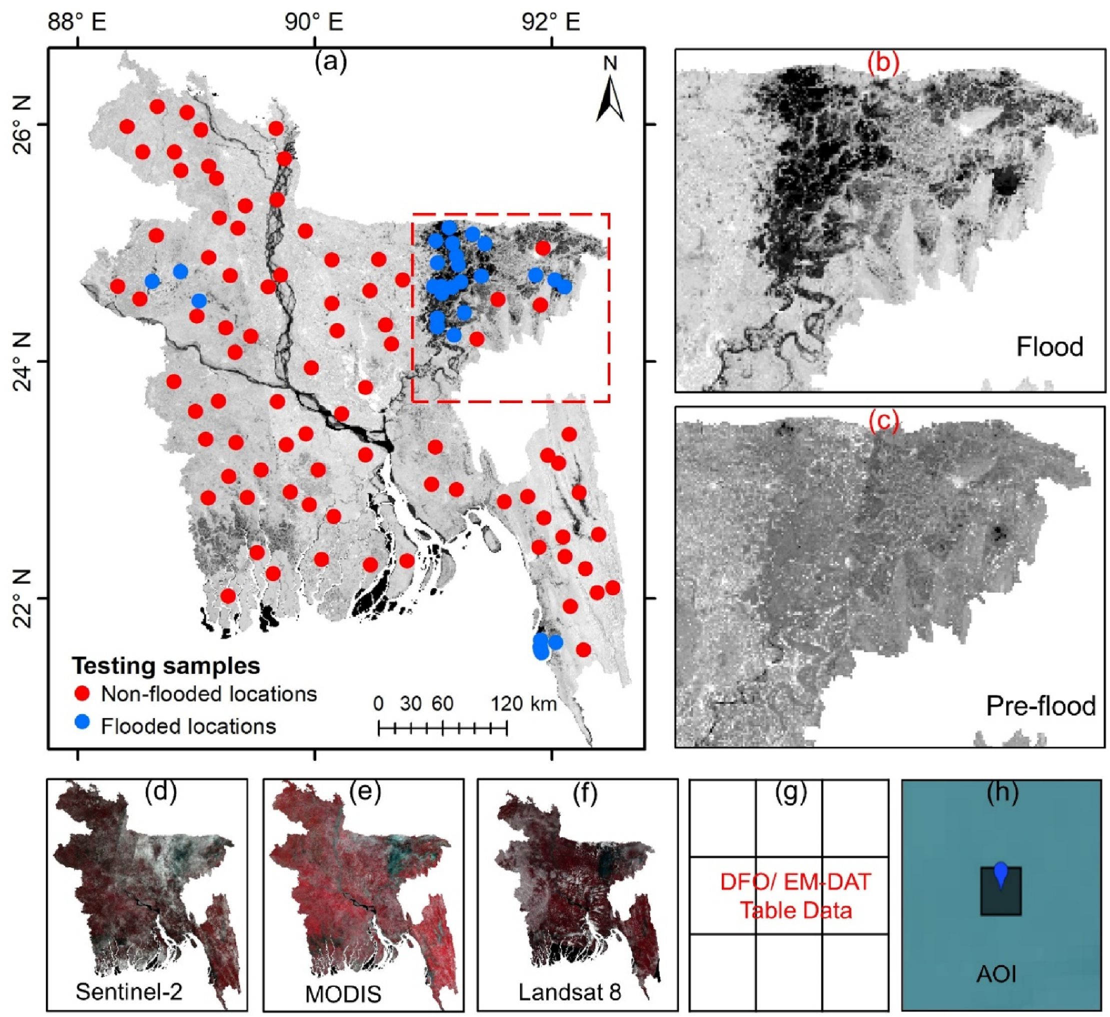

Fig. 5. Validation sample collection. (a) Sentinel-1 image composite for June 2018 overlaying with the collected sample locations. The testing samples were selected using the Sentinel-2, MODIS, Landsat 8, EM-DAT and DFO; (b) zoomed 'during flood' Sentinel-1 image composite of Bangladesh in June 2018; (c) zoomed 'pre-flood' Sentinel-1 composite image of Bangladesh acquired in March 2018; (d) Sentinel-2 false color composite (FCC); (e) MODIS FCC; (f) Landsat8 FCC; (g) DFO/EM-DAT table data representation; (h) AOI generation case. In the figure (b), dark areas indicate the floods.

inundation in the reference image.

2.3.3. Accuracy assessment and inter-comparison of flood maps

Accuracy assessment of our resultant flood maps includes two approaches: (1) a validation using the samples collected from multiple sources of flood events data and high/medium resolution satellite images and (2) a comparison with Sentinel-2 based flood maps.

Our study area was large, so to cover a reasonable area and to obtain correct validation samples, we collected the validation samples (reference data) using multiple datasets: (1) high resolution Sentinel-2 images, (2) Landsat 8 images, (3) MODIS images, (4) DFO datasets (flooded area with longitude and latitude), and (5) EM-DAT datasets (flooded area in general e.g. Sylhet district) (Fig. 5). We used the stratified random sampling approach to collect the validation samples. First, we divided the study area into six landcover classes (permanent water, floods, vegetation, cropland, built-up and others) according to the MODIS land cover map (Sulla-Menashe and Friedl, 2018) and Landsat-based JRC Monthly Water History data (Pekel et al., 2016). Second, we generated random sample points in each class and then we created area of interest (AOIs) as square buffers of those points (Dong et al., 2016). After experimenting with the several buffer sizes, we selected the 100 m × 100 m AOIs based on the collected sample points for validating the flood maps as it can provide a reasonable number of pure flooding pixels in each AOI. Third, we manually verified each of the AOIs and labelled them (flooded or non-flooded) in accordance to the above-mentioned multi-source datasets (Sentinel-2, MODIS, Landsat, EM-DAT, DFO). The AOIs without any confirmed signature of suitable classes (flood or non-flood) due to data quality issues such as clouds were excluded from the accuracy assessment. The AOI generation and validation were performed using the same monthly composited images when severe floods were reported in the DFO and EM-DAT datasets (Fig. 5). A total of 108, 93, 112, 109, and 113 AOIs were collected for 2014 (August), 2015 (June), 2016 (July), 2017 (August), and 2018 (June) respectively for the validation of flood maps (Supplementary Fig. 2). The total number of flooded and non-flooded pixels for each AOIs are provided in Supplementary Table 1. Finally, we calculated the confusion matrices (Congalton and Green, 2008) for the flood map to measure the accuracy of the results.

In addition to the validation, we compared the Sentinel-1 based flood maps with the Sentinel-2-based flood maps, previous studies (Hostache et al., 2012; Uddin et al., 2019), and agency generated maps (http://ffwc.gov.bd/index.php). Despite potential errors in identifying water and floods using optical imagery due to clouds, the relatively high temporal resolution can offset the effects of clouds to some degree (Clement et al., 2018). The normalized difference water index (NDWI) was used to extract the flooded area, which is calculated as follows:

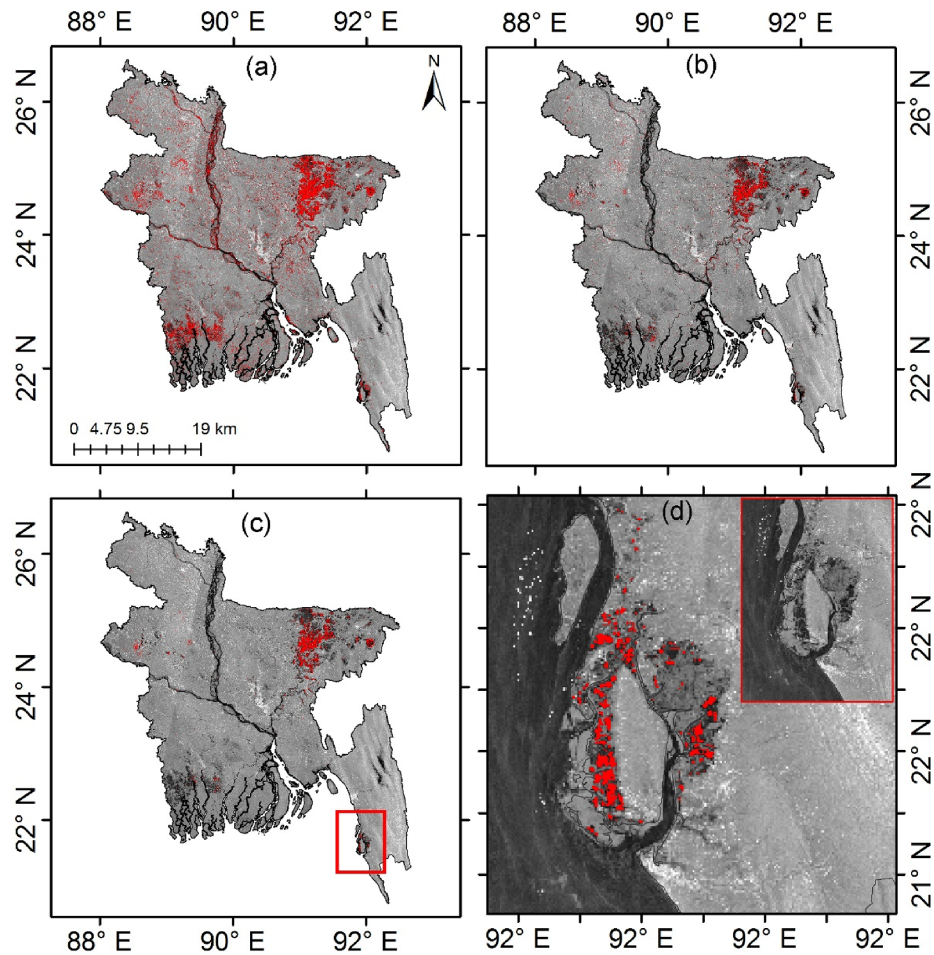

Fig. 6. Flooded areas derived from two algorithms and Sentinel-1 images in June 2018. (a) using CDAT algorithm; (b) using NDFI algorithm; (c) consistency map (flooded areas common for both the CDAT and NDFI algorithm; (d) zoomed area from the consistency map showing Cox's bazar flood.

$$NDWI = \frac{Green - NIR}{Green + NIR} \tag{3}$$

where *Green* and *NIR* are the reflectance of the green and near-infrared bands. NDWI highlights all the surface water bodies from the input time series Sentinel-2 datasets (Munasinghe et al., 2018). To extract the flooded areas, we removed the permanent water bodies using the dry season NDWI. The Sentinel-2 based flood map may not be perfect due to frequent clouds in the study area, but it served our purpose of evaluating the spatial pattern of SAR based flood maps.

3. Results

3.1. Accuracy assessment and inter-comparison of flooding maps from multiple sources

We used two flood detection algorithms (CDAT and NDFI) to generate consistent flood maps where floods were detected in both the algorithms (Fig. 6). Due to differences in the approach of the algorithms, discrepancies exist between the two results. However, the consistency map minimized uncertainties in the flood maps. The consistency maps were considered as actual flooding in our study. The zoomed consistency flood map in June 2018 could detect the deadly cox's bazar flood accurately (Fig. 6). We assessed the accuracy of the consistent flood maps using the collected reference samples (See Section 2.3.3). The validation based on the flooding events-based AOIs indicated that the produced flood maps had high accuracies (Table 2). The accuracies of the flood maps were not equal across the years; the overall accuracies were 84%, 87%, 90%, 85% and 92% in the 2014 (August), 2015 (June), 2016 (July), 2017 (August) and 2018 (June) respectively. The user's accuracy (UA) and producer's accuracy (PA) of the flood class were (UA, 73% and PA, 55%) in 2014; (UA, 100% and PA, 49%) in 2015; (UA, 88% and PA, 74%) in 2016; (UA, 100% and PA, 58%) in 2017 and (UA,100% and PA, 67%) in 2018. The high accuracy of our flood maps could be attributed to the combination of the two different algorithms. The combined results from the two algorithms increased the accuracy and certainty of the flood maps. The flood water pixels are distinct with very low backscatter coefficient and their identification from a SAR image is quite straight forward and less complex, and this could be another reason for the high accuracy of our flood map. The lowest accuracies were obtained in 2014 and 2017 (OA, 84% and 85%) when flooding areas were distributed in very smaller patches. The error might be associated with the estimation of threshold value and the low flood area proportion. For more uncertainty analysis please refer to the discussion Section 4.2. Overall, all of the five years of flood maps had reasonably good accuracies and can be used to quantify the dynamics of flood areas during 2014–2018. This study also indicates that the flood maps from our combined algorithm are reliable if there are sufficient numbers of observations of Sentinel-1 images.

The comparison of the flood maps and results from other satellite data in previous studies is important (Clement et al., 2018; Dottori et al., 2016; Hoque et al., 2011; Islam et al., 2010). Here, we also conducted a comparison between the Sentinel-1-based flood maps in this study and the results from the Sentinel-2 for 2014–2018. The comparison showed that the two maps agree highly and are spatially consistent in the frequently flooded areas. The Sentinel-1 SAR based

Table 2
Confusion matrix for accuracy assessment based on area of interest (AOIs) from multi-source satellite images and flood archive data.

Year (month)	Class	Non-flooded	Flooded	User's accuracy	Producer's accuracy	Overall accuracy
2014 (August)	Non-flooded	7712	516	0.86	0.93	0.84
	Flooded	1174	1467	0.73	0.55	
2015 (June)	Non-flooded	7053	0	0.86	1	0.87
	Flooded	1117	1100	1	0.49	
2016 (July)	Non-flooded	7916	298	0.91	0.96	0.90
	Flooded	774	2272	0.88	0.74	
2017 (August)	Non-flooded	7121	0	0.81	1	0.85
	Flooded	1599	2213	1	0.58	
2018 (June)	Non-flooded	8366	0	0.90	1	0.92
	Flooded	886	1996	1	0.67	

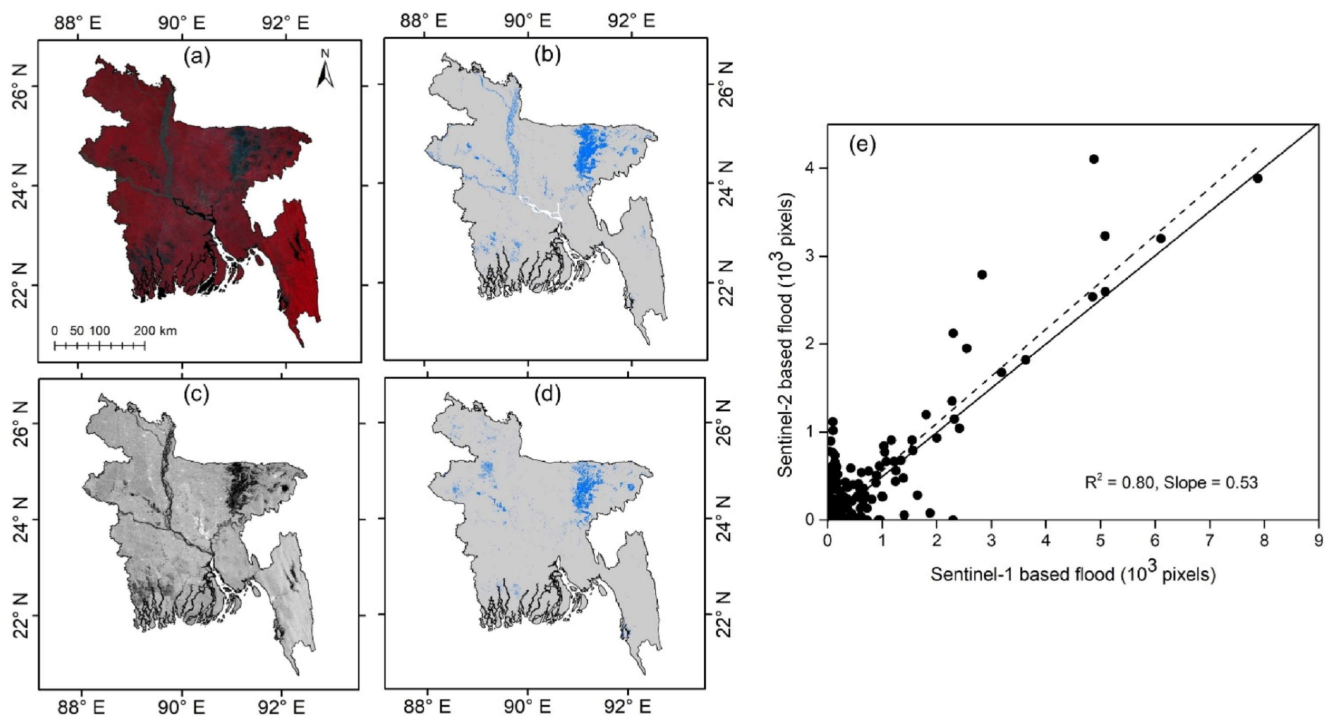

Fig. 7. Spatial pattern comparison between Sentinel-1 and Sentinel-2 flood maps. (a) Sentinel-2 false color composite using bands red, near infra-red, and green bands; (b) Sentinel-2 derived flood; (c) Sentinel-1 composite of VV band; (d) Sentinel-1 derived flood. The maps were derived for the year 2018, and the comparison is only for general purpose to visualize and check the spatial consistency; (e) scatter plot for the comparison between Sentinel-1 based and Sentinel-2 based flood area at sub-district level in 2018.

results were more detailed, and in particular it could exclude roads and small houses which were not flooded with its 10 m spatial resolution. The high temporal resolution (6 or 12 days) of Sentinel-1 allowed for the rapid mapping of floods events. Additionally, Sentinel-1 has a higher capacity to accurately map flooding in the cloudy conditions of sub-tropical Bangladesh during the rainy season. Fig. 7 shows the spatial comparison between Sentinel-1 SAR-based flood map and Sentinel-2 based flood map. The comparison of flooded area estimates at the sub-district level between the Sentinel-1 based and Sentinel-2 based flood map was significantly correlated with the R^2 value of 0.8 (Fig. 7e). However, the Sentinel-2 based flood map underestimated flood area due to the lack of data induced by cloud cover during rainy periods of floods. We also compared our results with existing studies (Hoque et al., 2011; Islam et al., 2010; Uddin et al., 2019) and with the reports from the Flood Forecasting and Warning Centre of Bangladesh Water Development Board (BWDB) (http://ffwc.gov.bd/index.php). Our flood maps had a high spatial consistency with the existing flood maps. The validation and comparison with existing products indicated that the flood maps generated in our study are reliable.

3.2. Spatiotemporal pattern of floods

The spatial extent and the progression of flood was observed and analyzed from the monthly time series Sentinel-1 based flood maps. The analysis of flood maps showed that the flooded area was large and extensive for Bangladesh. The maximum flooded area during monsoon season (June to September) varied approximately between 7,112 km^2 and 12,040 km^2 in Bangladesh during 2015–2018. During the study period, the annual maximum and minimum flooded areas occurred in 2015 and 2018, respectively, and the monsoon season maximum and minimum flooded area was in 2018 and 2015, respectively. The flood maps are shown only for the rainy season of the year except for the 2014 where only October, November, and December acquisition was available (Fig. 8). The monthly flooding maps are provided in the Supplementary Fig. 3. During the peak flooding stage, the flooded area covers approximately 8% of Bangladesh. During 2014–2018, for each year about 6% of the country was inundated by flood water. Flooding often occurred in the monsoon season, however excess pre-monsoon rainfall caused occasional floods in some regions (Supplementary Table 2, Supplementary Fig. 4).

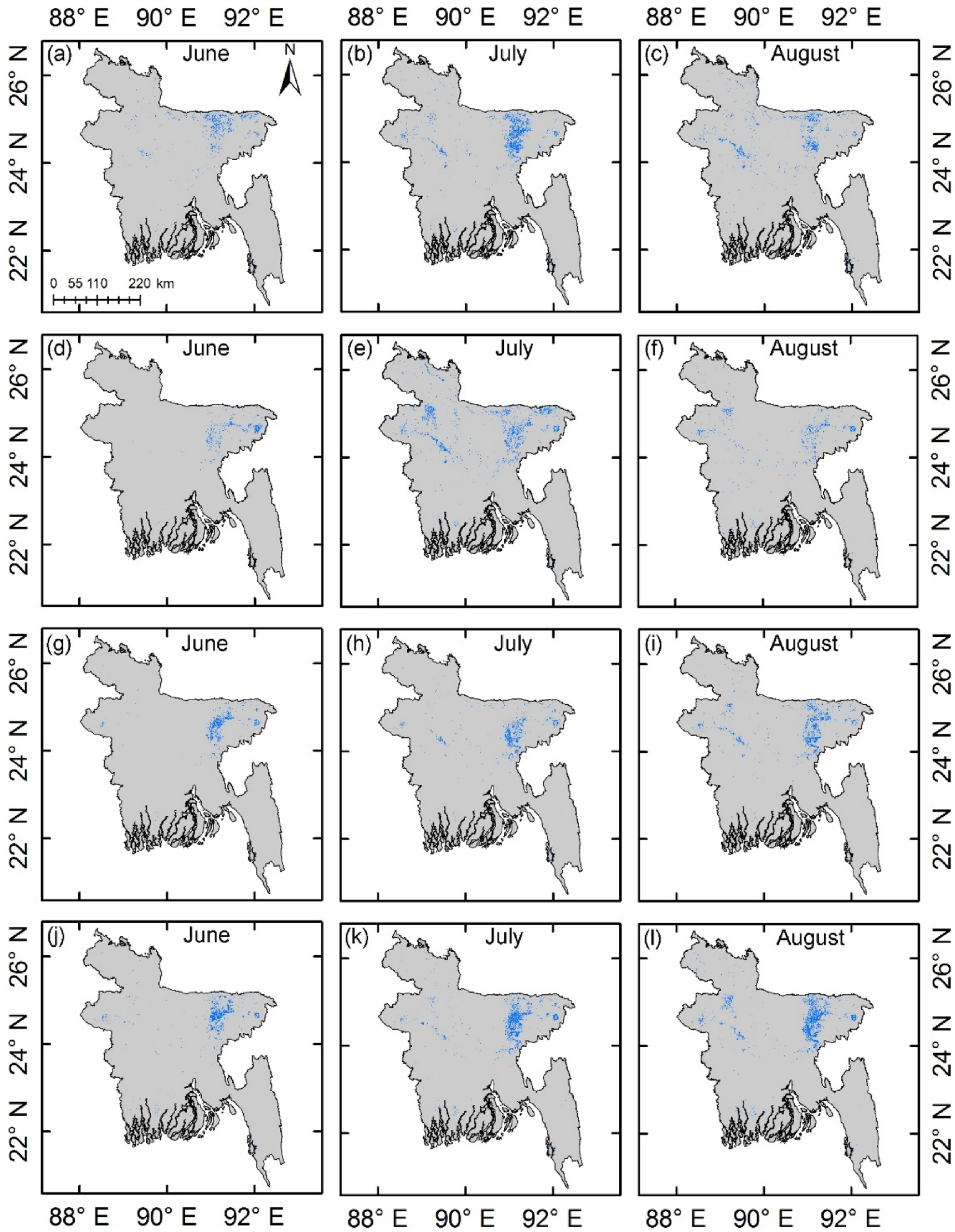

Fig. 8. Flooding pattern in rainy season (June-August) during 2015–2018. (a-c) 2015, (d-f) 2016, (g-i) 2017, (j-l) 2018.

Extensive flooding occurred in the Meghna River basin in northeastern Bangladesh, where floods happened every year. The time series flood maps revealed that the flood in this region of Bangladesh occurred in the early rainy season and the flood water remained for a longer period than other areas. The other regions of the country only flooded if experienced excess or extreme precipitation during the year. The peak flood month usually occurred between July and September, coinciding with the highest monsoon rainfall with the respective year. In early October, flood water starts to retreat back to the normal stage, beginning from the far away areas to the areas nearest of lakes and rivers. Extreme rainfall events in the catchments of Ganges, Brahmaputra, and Meghna Rivers can lead to floods at any time during the monsoon season, leaving short term and shallow flooded areas. With the exception of the monsoon and pre-monsoon extreme rainfall, if flooding occurs it is usually due to man-made controlled flooding for paddy rice cultivation or is due to tides or storms. The seasonality of the flooding time has direct impacts on the agrarian economy of Bangladesh, where paddy rice is often cultivated thrice in a year. The yield of the paddy rice highly depends on the flooding time period, as unlike the other crops, the paddy rice is primary cultivated in inundated lands. The progression of the flood starts along the river in the lowland areas to the elevated regions with the surplus rainfall in the basin and the upper catchments of the rivers. We showed the pattern of flooding from Sentinel-2 for the year 2018 in Fig. 9, which shows normal versus flooding season and helps us visualize the flood dynamics and changes in a year. The Sentinel-2 false color composite (FCC) of the dry season depicts normal conditions with permanent waters and no sign of any flooding (Fig. 9a), and the corresponding NDWI shows the permanent waters more clearly (Fig. 9c). The FCC of the wet season shows the flooded conditions, clearly visible in the northeast of Bangladesh (Fig. 9b), the flooded areas are prominent in the corresponding NDWI image (Fig. 9d). These contrasting images of dry and wet conditions show us the severity and extensiveness of floods in Bangladesh. Fig. 10 demonstrates a zoom in of flooding events for random locations in

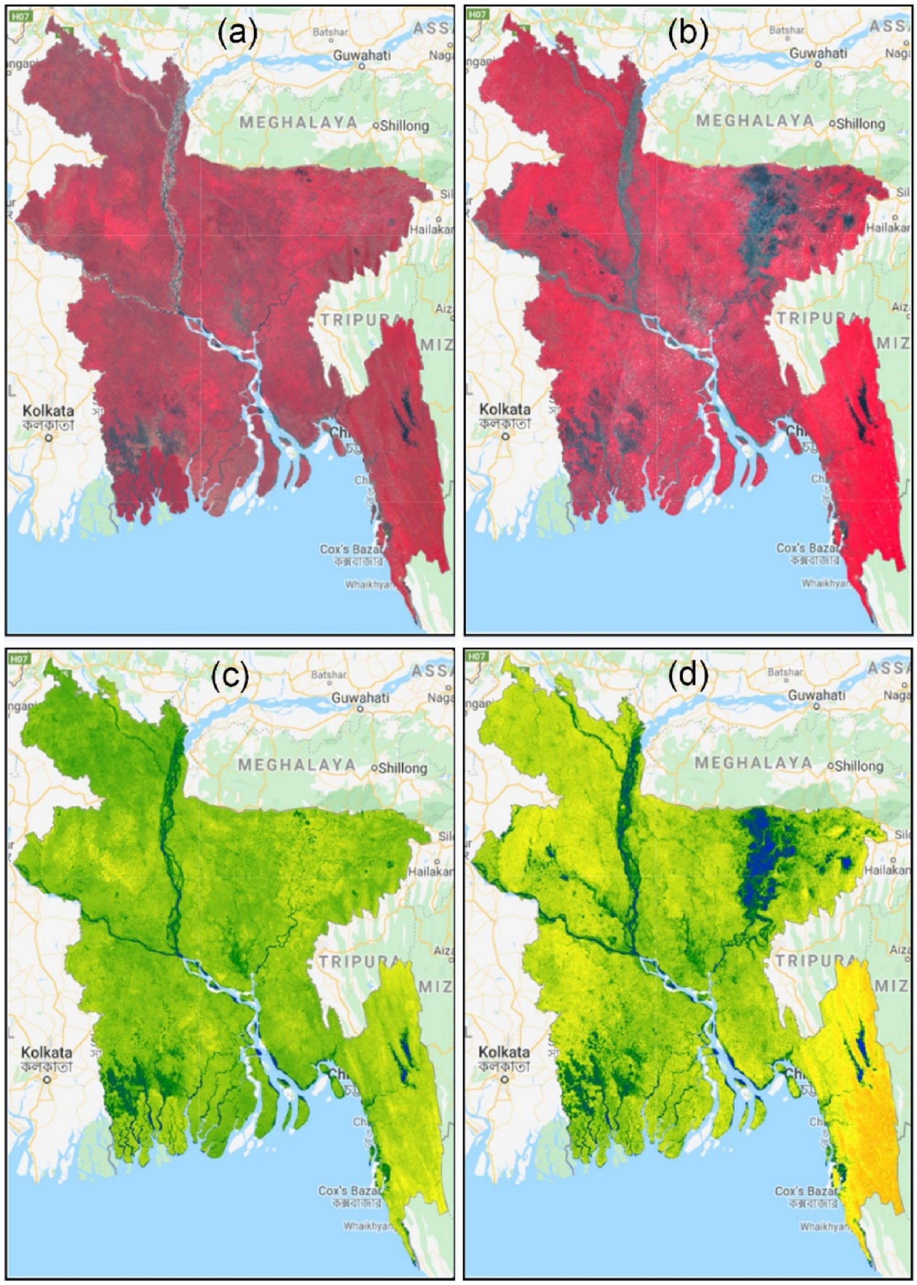

Fig. 9. Flooding pattern depicted from Sentinel-2 in 2018 using the red, near infra-red, and green bands. (a) Sentinel-2 false color composite from the dry season (January to April); (b) Sentinel-2 false color composite from the rainy season (June to August); (c) flooding pattern in the dry season (January to April); (d) flooding pattern in the rainy season (June to August). Flooding is shown in dark blue. (For interpretation of the references to color in this figure legend, the reader is referred to the web version of this article.)

Bangladesh. The zoomed images indicate that floods occurred in large areas and in small fragmented areas.

3.3. Flood frequency characteristics and flooding hotspots

Flood frequency depicts how often an area is inundated during the observed period and frequent flooding hotspots. Fig. 11 shows the flooding frequency of Bangladesh for 2014–2018. The frequently flooded areas are located near the river or water bodies. The Ganges, Brahmaputra, and Meghna River basins get flooded frequently with a high discharge of waters from these three rivers and their tributaries. An area of approximately 28,586 km^2 was flooded five times, representing every year of flooding in those areas in 2014–2018. An area of 207,762 km^2 as flooded once during 2014–2018. The most often flooded region was the northeast and northwest states of Sylhet and Rajshahi (Fig. 11). Along with the extreme rainfall, the Bangladesh flooding highly depends on the excess water flows from the upper catchment of the Ganges, Brahmaputra, and Meghna River basins. Cherrapunji, the world's highest rainfall region is situated north to the Bangladesh and most of its downfall flows directly into the flat land of Bangladesh causing severe floods almost every year. Characteristically, the northeastern Sylhet region of Bangladesh near to the Cherapunji get flooded every year in the early monsoon season and suffers the longest flooding period. It can be observed that in the frequently flooded regions, flood water overflows through the roads or settlements (Fig. 10). The less flooded regions are slightly elevated lands. The coastal region was identified as less flooded, due to dense mangrove forest of Sundarbans and floods under vegetation may not detected unless they are

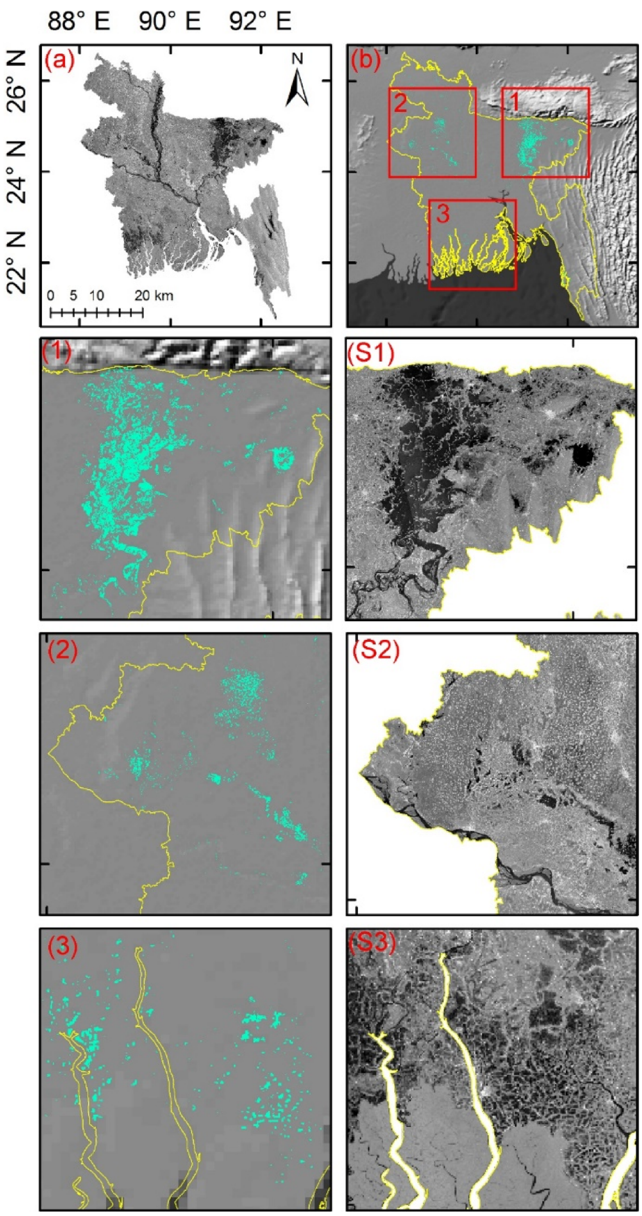

Fig. 10. Detailed flood maps. (a) The Sentinel-1 SAR composite of Bangladesh in August 2018; (b) and resultant flood map; (1) - (3) the zoom in maps show local details of flooding in various locations; (S1-S3) respective Sentinel-1 zoom in.

very severe.

The long term (1986–2015) flooded area derived from the Landsat monthly surface water showed similar patterns (Fig. 11b). These long-term flooded areas are the ratio in percentage between the flood counts and total Landsat observations. Except in northeastern Sylhet, the areas along the Padma River also flooded often, evident from this long-term analysis. The yearly flood frequency obtained from the Sentinel-1 was provided in the Supplementary Fig. 5. The long-term flood frequency indicates that the regions that are likely to be flooded remain unchanged for the last 30 years. Therefore, increasing the flood protection standard and adaption are the key to decrease the devastating impact of floods in these regions.

3.4. Flood-affected paddy rice fields

The flood-affected paddy rice planting areas are shown in Fig. 12. The paddy rice maps were overlaid on the flood maps to determine the rice cultivated areas affected by floods in 2014–2018. Annual floods typically threatened the paddy rice planting areas, because a vast majority of rice croplands are in the low river deltas in Bangladesh. The flood season (May to October) corresponds to the harvesting of Boro rice (December-May) and the growing periods of Aus rice (April-August) and Aman rice (July-November). The paddy rice areas affected by flood ranges approximately from 1.61% to 18.17% of the total rice areas during the study period (Fig. 12g). In general, paddy rice areas affected by floods were between approximately 1,018–11,436 km^2 in 2014–2018. The results indicated that the flood affected regions are the lowland areas of the Ganges, Brahmaputra, and Meghna River basins. The most often flood-affected paddy rice areas were concentrated in the northeast and northwest states of Sylhet and Rajshahi. The paddy rice areas near to the rivers or streams are found to be more vulnerable to the floods. It was observed that paddy rice areas are under constant threat to floods throughout the year. The impact of floods on paddy rice depended on the severity and longevity of floods as well as the rice growth stage. Floods are usually more harmful when the rice plants are between the flowering and maturity stages. The size of the exposed paddy rice area to floods will increase in the future with the expansion of cropland areas, and increasing paddy rice cropping intensity (FAOSTAT, 2019). The damage caused by flood to the rice agriculture has an immense negative impact on local communities and the GDP of the country. Knowledge of the spatial distribution of flood-affected paddy rice planting areas is important for effective crop management to avoid possible reduction of rice production.

4. Discussion

Extensive and frequent flooding is a profound problem of Bangladesh. Annually, on average, floods cause economic losses equivalent to 1.5% of gross domestic product (GDP). In the past, some efforts have been made to map flooding extent in Bangladesh (Ahmed et al., 2017; Hoque et al., 2011; Islam et al., 2010; Uddin et al., 2019) to assess the flood impacts. However, these efforts were performed for small regions and a nationwide understanding of flooding and its dynamics were not reported. Due to the limited availability of cloud-free images during flood events, often the maps generated from the optical sensors underestimated flood area for key flooding events. Most of the studies generated flood maps for a single month, however floods have lasted longer than a month on several occasions. Annual and recent flooding maps were also unavailable for Bangladesh as the researchers tend to publish the flood map results a few years after the flood events. In our study, we addressed these issues by generating nationwide monthly flood maps for 2014–2018 using the cloud independent SAR data and the cloud computing GEE platform. Using our methods, we were able to generate recent flood maps as soon as Sentinel-1 data are available. Additionally, we detected the flood-affected paddy rice areas to further aid pre- and post-flood management to minimize the economic losses caused by floods and maintain the nation's food security.

4.1. Reliability of flood mapping using all the available Sentinel-1 imagery, integrating two algorithms, and GEE

This study demonstrated an operational approach to large-scale flood mapping by integrating long time series SAR imagery, a combination of CDAT and NDFI algorithms, and parallel computing facilities. Through the spatiotemporal analysis of annual flood maps derived from the Sentinel-1 SAR, we found that floods occur almost every year in the monsoon season. The yearly flooded areas were consistent with the previous reporting in Bangladesh (Hoque et al., 2011; Islam et al., 2010).

Sentinel-1 provides rapid image acquisitions, generates dense time series data, and facilitates near–real time flood mapping and monitoring. With the all-weather capability of SAR, it provides enough number of acquisitions to meet the observation requirement for

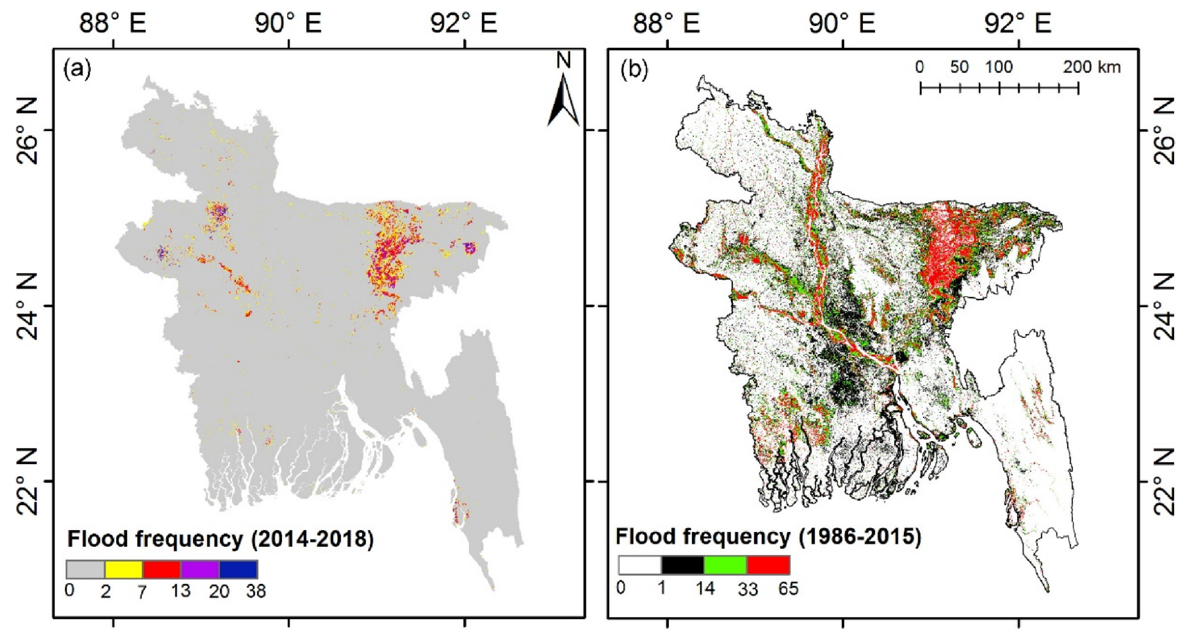

Fig. 11. Recent and long-term flood frequency of Bangladesh. (a) Sentinel-1-derived flood frequency (count) between 2014 and 2018, (b) Landsat-based long-term flood frequency (percent) between 1986 and 2015.

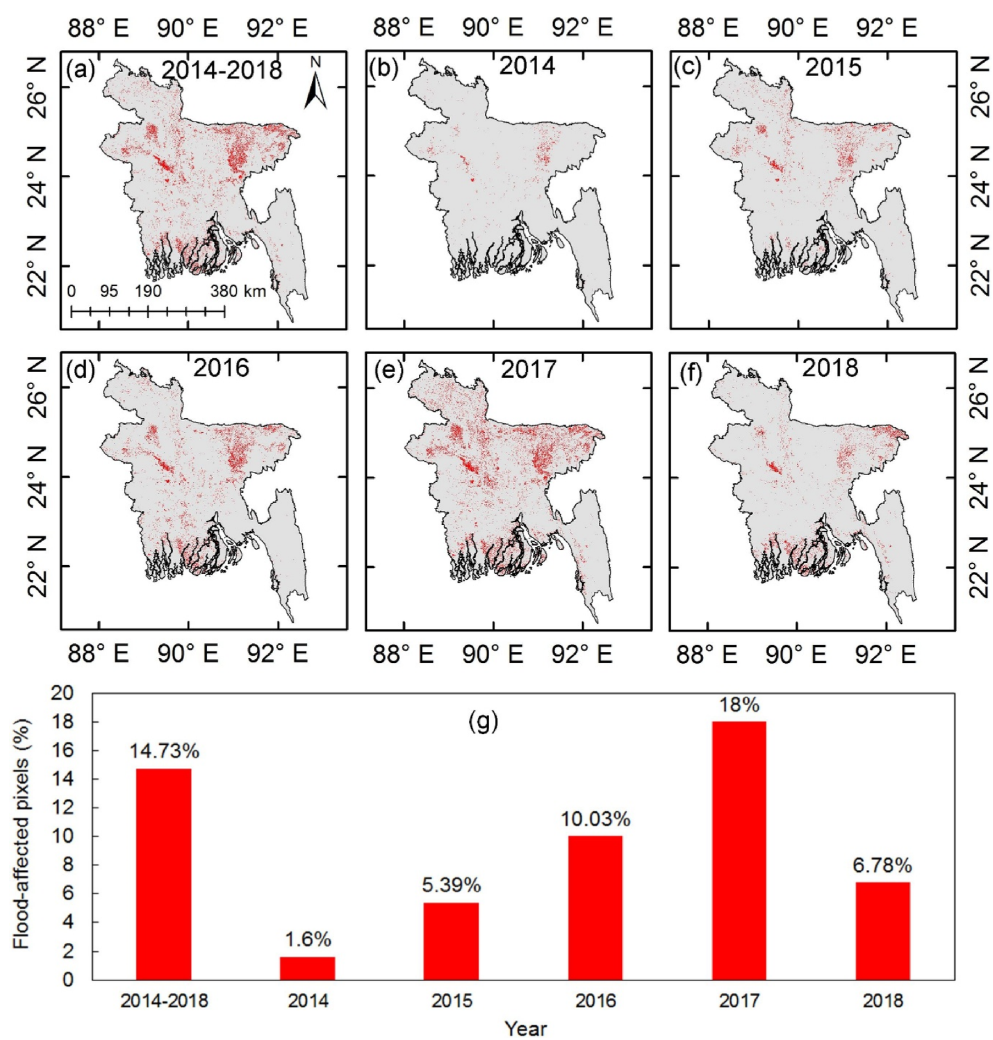

Fig. 12. Paddy rice planting areas affected by floods. (a) 2014–2018; (b) 2014; (c) 2015; (d) 2016; (e) 2017; (f) 2018 and (g) percentage of total paddy rice pixels affected by flood.

monthly mapping of floods for the entirety of Bangladesh. The floods were determined by the CDAT and NDFI algorithms, these algorithms were developed using high temporal resolution SAR data (Long et al., 2014). Our methods identified flooded areas based on the difference of pre- and post-flood images and threshold values were determined from the statistics and applied to the differenced images. This method allows for the identification of flooded areas for each individual image and can be used for automatic, near real-time flood identification (Long et al., 2014). Our study demonstrated an effective way of using all the available Sentinel-1 imagery and the algorithm that particularly designed for effective flood identification.

Floods mainly occur in the rainy season during a time with extensive cloud cover. The cloud-independent Sentinel-1 SAR took full advantage of the image acquisitions unhampered by cloud contaminated pixels. This work shows the reliability of creating accurate flooding maps by obtaining enough observations during the flooding time, particularly in Asia. The C-band SAR is unable to penetrate through the dense forest omitting many water pixels. This problem probably influenced the flood detection in southern Bangladesh where dense mangrove forests are present. However, most of Bangladesh consists of flat croplands and flooding under vegetation is not extensive.

The GEE platform hosts all the available Sentinel-1 SAR images at a petabyte scale and provides high-performance parallel computation facilities (Gorelick et al., 2017). It provides pre-processing of Sentinel-1 data up to the terrain-corrected level, reducing the time requirement of intense pre-processing steps of raw Sentinel-1 data. GEE provides opportunities for not only traditional remote sensing communities but also other scientists who lack the technical experience to handle large scale microwave data, supercomputers, and cloud computing facilities. Quick responses to flood affected areas are very important. Here, we demonstrated that a huge amount of SAR data for a large area can be used to detect flooded regions very quickly. Thus, our approach can also be used for other regions of the world, making near real-time monitoring of flood waters a possibility after some further tests in other regions.

Several efficient and accurate flood detection algorithms are available based on microwave data. Although these algorithms are based on various techniques and have various complexity, their resultant flood maps are not substantially different. The choice of the algorithm depends on its complexity of implementation and accuracy. For our study, we used two recently developed flood detection algorithms (CDAT and NDFI). These two algorithms were selected for the following reasons: (1) CDAT and NDFI both are simple to implement and efficient for rapid and quick flood mapping; (2) these algorithms can be extended to other regions very easily with minimum required changes; (3) they have potential for automatic flood mapping; and (4) these algorithms produced accurate flood maps for a large area (country scale). We considered the areas commonly detected by both the algorithms as a flooded area in our study to reduce the uncertainty in the results. Both algorithms could detect the major flooding events in the study area with similar spatial patterns. The differences existed in the results generated by the two algorithms were primarily in small and shallow flooded areas. The amalgamated approach used in this study significantly reduces the false flood alarm that could be an initial step towards a large-scale automatic flood monitoring system in the future.

4.2. Uncertainty analyses

All the available Sentinel-1 imagery is useful for large-scale rapid flood mapping and monitoring in Bangladesh. However, some uncertainties exist in the flood maps generated from Sentinel-1. First, the uncertainty of flood extent maps could be from the sparse temporal resolution of Sentinel-1, usually 6–12 days depending on the location (Geographical Coverage, 2018). As flood water changes rapidly, this temporal resolution may not be sufficient to track flood progression. This is worsened when considering a large area such as Bangladesh, where accurate identification of the high flood stages or the maximum extent became a challenge. Second, uncertainty arises in the SAR-based flood areas due to the environmental conditions of the study regions, such as the presence of winds at the time of the image acquisition, topography, vegetation types, and built-up areas. All of them could have influence on the results to some degree. Winds roughs the water surfaces and disturb the specular reflection characteristics of water, and can cause an inaccurate determination of flooded areas. The radar shadow generated from the hilly terrain creates misclassification of surface water that might lead to overestimation of flooded areas. The flood water under vegetation cover could not be detected with the C-band Sentinel-1 SAR, while L-band data, for example the Phased Array type L-band (PALSAR) (Rosenqvist et al., 2007) SAR, might provide information under vegetation for flood mapping. The identification of flooded locations within urban areas are hampered by the double bounce of radar signals from buildings. However, high-resolution SAR images (e.g. Sentinel-1) have demonstrated some promising results and the effects of these factors are negligible. Third, the flood areas depended on the selection of threshold values and the choice of these values may induce an under or overestimation of the flood area. Though the threshold values were selected based on the suggested and experimented values, they may limit the ability to detect all the flooded locations. Finally, selection of the non-flooded reference SAR images can influence the detection of the flooded areas. The seasonal variations in land cover and differences in Sentinel-1 acquisition parameters could lead to differences in the SAR signals for the water areas for the same location in varying time periods.

Using the Sentinel-1 data alone, it is not completely possible to differentiate the individual events that influence flooding. The ancillary data related to the dykes and river gauge can help to distinguish the flooding components more reliably. Bangladesh is a major rice production country, where rice transplanting-related flooding is common for irrigation of paddy rice fields. This phenomenon should be considered for the flood modeling in the Bangladesh.

4.3. Challenges and implications for flood mitigation in Bangladesh

Water related disasters are a common phenomenon in Bangladesh and living with flood is not an option but a way of life (Ali et al., 2019). Almost every location in Bangladesh is affected by floods with varying frequency and intensity. Floods in Bangladesh could be related to river overflow, human controlled water release, and/or extreme rainfall and tides. Flood extent and timing is a complex combination of these events, including excess rainfall in the upstream basin (Kuenzer et al., 2013). The flooding in Bangladesh depends on the total precipitation in the Ganges, Brahmaputra, and Meghna River basins. Extreme flooding events occurred when the peak water-flow of these river exceeds certain thresholds (Ali et al., 2019).

Every year flood causes approximately 2 billion USD (Ali et al., 2019) of damage in Bangladesh, primarily due to agricultural losses. In the future with the changing climate, it is expected that the intensity and frequency of flooding will increase and that the low-lying areas will become more at risk of extreme flooding. Bangladesh is densely populated (more than 1,000 person/ km^2) and continuous private and public development is happening in low-lying areas, which will further increase the scale of damage and loss of lives when extreme flooding occurs. The long-term economic loss caused by floods has hampered development goals set by the government. Flood management is a challenging task due to its unavoidable nature, complexity, and scale. To mitigate the regular flooding events, existing structural and non-structural prevention measures are not sufficient for Bangladesh. To lessen the impact of floods, the local and central governments need to develop and deploy appropriate flood early warning systems and disseminate flooding information via modern communication systems such as cell phones. The government must have an efficient flood management plan and should focus on increasing local flood protection standard as a prevention measure.

5. Conclusions

Previous efforts on SAR based-flood mapping generally focused on small areas. Thus, our knowledge of the annual progression of floods, their extent, and its impact is limited in Bangladesh, one of the most flood-prone countries in Asia. Using all the available Sentinel-1 SAR data during 2014–2018, the improved CDAT and NDFI algorithms, and the Google Earth Engine (GEE), we generated high resolution (10-m) monthly flood maps of Bangladesh for 2014–2018. To our knowledge, this is the first application of Sentinel-1 imagery in flood mapping for the entire country of Bangladesh. The results showed that flood is frequent in northeastern Bangladesh and along the pathways of the three major rivers: the Ganges, Brahmaputra, and Meghna. Our study also demonstrated the potential of the GEE cloud-computing platform for mapping using large-scale high-resolution SAR imagery. With the high cloud cover during the flooding season in tropical regions, the cloud-independent Sentinel-1 satellite has been proved effective in mapping and monitoring floods at a high spatial and temporal resolution.

The generated flood maps will be helpful for disaster management agencies, policy makers, and government agencies that respond to flood disasters and aim to mitigate and prevent flooding. We also used the flood observations to identify the paddy rice areas that were affected by floods. The existing paddy rice planting areas in these regions were found to be very prone to severe flooding events. The estimated flood affected rice area is helpful to the government for post-flood compensation, restoration efforts, and monitoring purposes. Despite the reliability of our demonstrated approach, we would encourage to conduct a thorough evaluation of the proposed method prior to applying it to other regions. In the future, the inclusion of river gauge data can be explored to improve flood mapping and better determine rice areas affected by floods.

Declaration of Competing Interest

The authors declare that they have no known competing financial interests or personal relationships that could have appeared to influence the work reported in this paper.

Acknowledgements

This study is funded by the National Natural Science Foundation of China (No. 41871349), the Key Research Program of Frontier Sciences (QYZDB-SSW-DQC005) and the Strategic Priority Research Program (XDA19040301) of Chinese Academy of Sciences (CAS). Mrinal Singha acknowledges CAS President's International Fellowship Initiative (PIFI) for providing the fellowship to carry out this research.

Appendix A. Supplementary material

Supplementary data to this article can be found online at https://doi.org/10.1016/j.isprsjprs.2020.06.011.

References

Adikari, Y., Yoshitani, J., 2009. Global trends in water-related disasters: an insight for policymakers. World Water Assessment Programme Side Publication Series, Insights. The United Nations, UNESCO. International Centre for Water Hazard and Risk Management (ICHARM).
Ahmed, M.R., Rahaman, K.R., Kok, A., Hassan, Q.K., 2017. Remote sensing-based quantification of the impact of flash flooding on the rice production: a case study over Northeastern Bangladesh. Sensors 17, 2347.
Ali, M.H., Bhattacharya, B., Islam, A.S., Islam, G.M.T., Hossain, M.S., Khan, A.S., 2019. Challenges for flood risk management in flood-prone Sirajganj region of Bangladesh. J. Flood Risk Manage. 12, e12450.
Amitrano, D., Di Martino, G., Iodice, A., Riccio, D., Ruello, G., 2018. Unsupervised rapid flood mapping using Sentinel-1 GRD SAR images. IEEE Trans. Geosci. Remote Sens. 56, 3290–3299.
Arnell, N.W., Gosling, S.N., 2016. The impacts of climate change on river flood risk at the global scale. Clim. Change 134, 387–401.
Bangladesh, 2019. Ricepedia. accessed 6.2.19. http://ricepedia.org/bangladesh.
Brisco, B., Short, N., van der Sanden, J., Landry, R., Raymond, D., 2009. A semi-automated tool for surface water mapping with RADARSAT-1. Canadian J. Remote Sens. 35, 336–344.
Cian, F., Marconcini, M., Ceccato, P., 2018. Normalized Difference Flood Index for rapid flood mapping: taking advantage of EO big data. Remote Sens. Environ. 209, 712–730.
Clement, M.A., Kilsby, C.G., Moore, P., 2018. Multi-temporal synthetic aperture radar flood mapping using change detection. J. Flood Risk Manage. 11, 152–168.
Congalton, R.G., Green, K., 2008. Assessing the Accuracy of Remotely Sensed Data: Principles and Practices. CRC Press.
Dong, J., Xiao, X., Menarguez, M.A., Zhang, G., Qin, Y., Thau, D., Biradar, C., Moore III, B., 2016. Mapping paddy rice planting area in northeastern Asia with Landsat 8 images, phenology-based algorithm and Google Earth Engine. Remote Sens. Environ. 185, 142–154.
Doocy, S., Daniels, A., Murray, S., Kirsch, T.D., 2013. The human impact of floods: a historical review of events 1980–2009 and systematic literature review. PLOS Curr. Disast. 1.
Dottori, F., Salamon, P., Bianchi, A., Alfieri, L., Hirpa, F.A., Feyen, L., 2016. Development and evaluation of a framework for global flood hazard mapping. Adv. Water Resour. 94, 87–102.
FAOSTAT, 2019. FAOSTAT. accessed 12.9.19. http://www.fao.org/faostat/en/#data.
Funk, C., Peterson, P., Landsfeld, M., Pedreros, D., Verdin, J., Shukla, S., Husak, G., Rowland, J., Harrison, L., Hoell, A., 2015. The climate hazards infrared precipitation with stations—a new environmental record for monitoring extremes. Sci. Data 2, 150066.
Geographical Coverage, 2018. Geographical Coverage - Sentinel-1 - Sentinel Online. accessed 9.6.18. https://sentinel.esa.int/web/sentinel/missions/sentinel-1/satellite-description/geographical-coverage.
Gorelick, N., Hancher, M., Dixon, M., Ilyushchenko, S., Thau, D., Moore, R., 2017. Google Earth Engine: planetary-scale geospatial analysis for everyone. Remote Sens. Environ. 202, 18–27.
Hoque, R., Nakayama, D., Matsuyama, H., Matsumoto, J., 2011. Flood monitoring, mapping and assessing capabilities using RADARSAT remote sensing, GIS and ground data for Bangladesh. Nat. Hazards 57, 525–548.
Hostache, R., Chini, M., Giustarini, L., Neal, J., Kavetski, D., Wood, M., Corato, G., Pelich, R.-M., Matgen, P., 2018. Near-real-time assimilation of SAR-derived flood maps for improving flood forecasts. Water Resour. Res. 54, 5516–5535.
Hostache, R., Matgen, P., Wagner, W., 2012. Change detection approaches for flood extent mapping: how to select the most adequate reference image from online archives? Int. J. Appl. Earth Obs. Geoinf. 19, 205–213.
Huang, C., Chen, Y., Wu, J., 2014. Mapping spatio-temporal flood inundation dynamics at large river basin scale using time-series flow data and MODIS imagery. Int. J. Appl. Earth Obs. Geoinf. 26, 350–362.
Islam, A.S., Bala, S.K., Haque, M.A., 2010. Flood inundation map of Bangladesh using MODIS time-series images. J. Flood Risk Manage. 3, 210–222.
Jackson, K.R., Ramakrishnan, L., Muriki, K., Canon, S., Cholia, S., Shalf, J., Wasserman, H.J., Wright, N.J., 2010. Performance analysis of high performance computing applications on the amazon web services cloud. In: 2nd IEEE International Conference on Cloud Computing Technology and Science. IEEE, pp. 159–168.
Kuenzer, C., Guo, H., Huth, J., Leinenkugel, P., Li, X., Dech, S., 2013. Flood mapping and flood dynamics of the Mekong Delta: ENVISAT-ASAR-WSM based time series analyses. Remote Sensing 5, 687–715.
Li, S., Sun, D., Goldberg, M.D., Sjoberg, B., Santek, D., Hoffman, J.P., DeWeese, M., Restrepo, P., Lindsey, S., Holloway, E., 2018. Automatic near real-time flood detection using Suomi-NPP/VIIRS data. Remote Sens. Environ. 204, 672–689.
Long, S., Fatoyinbo, T.E., Policelli, F., 2014. Flood extent mapping for Namibia using change detection and thresholding with SAR. Environ. Res. Lett. 9, 035002.
Maclean, J., Hardy, B., Hettel, G., 2013. Rice Almanac: Source Book for One of the Most Important Economic Activities on Earth. IRRI.
Malenovský, Z., Rott, H., Cihlar, J., Schaepman, M.E., García-Santos, G., Fernandes, R., Berger, M., 2012. Sentinels for science: Potential of Sentinel-1,-2, and-3 missions for scientific observations of ocean, cryosphere, and land. Remote Sens. Environ. 120, 91–101.
Manfreda, S., Di Leo, M., Sole, A., 2011. Detection of flood-prone areas using digital elevation models. J. Hydrol. Eng. 16, 781–790.
Martinis, S., Kersten, J., Twele, A., 2015. A fully automated TerraSAR-X based flood service. ISPRS J. Photogramm. Remote Sens. 104, 203–212.
Martinis, S., Plank, S., Ćwik, K., 2018. The use of Sentinel-1 time-series data to improve flood monitoring in arid areas. Remote Sens. 10, 583.
Martinis, S., Twele, A., Voigt, S., 2009. Towards operational near real-time flood detection using a split-based automatic thresholding procedure on high resolution TerraSAR-X data. Nat. Hazards Earth Syst. Sci. 9, 303–314.
Mason, D.C., Davenport, I.J., Neal, J.C., Schumann, G.J.-P., Bates, P.D., 2012. Near real-time flood detection in urban and rural areas using high-resolution synthetic aperture radar images. IEEE Trans. Geosci. Remote Sens. 50, 3041–3052.
Mason, D.C., Speck, R., Devereux, B., Schumann, G.J.-P., Neal, J.C., Bates, P.D., 2010. Flood detection in urban areas using TerraSAR-X. IEEE Trans. Geosci. Remote Sens. 48, 882–894.
Matgen, P., Hostache, R., Schumann, G., Pfister, L., Hoffmann, L., Savenije, H.H.G., 2011. Towards an automated SAR-based flood monitoring system: lessons learned from two case studies. Phys. Chem. Earth, Parts A/B/C 36, 241–252.
Mirza, M.M.Q., 2002. Global warming and changes in the probability of occurrence of floods in Bangladesh and implications. Global Environ. Change 12, 127–138.
Munasinghe, D., Cohen, S., Huang, Y.-F., Tsang, Y.-P., Zhang, J., Fang, Z., 2018. Intercomparison of satellite remote sensing-based flood inundation mapping

techniques. JAWRA J. Am. Water Resour. Assoc. 54, 834–846.
Nemani, R., Votava, P., Michaelis, A., Melton, F., Milesi, C., 2011. Collaborative supercomputing for global change science. Eos, Trans. Am. Geophys. Union 92, 109–110.
Notti, D., Giordan, D., Caló, F., Pepe, A., Zucca, F., Galve, J., 2018. Potential and limitations of open satellite data for flood mapping. Remote Sens. 10, 1673.
Ouled Sghaier, M., Hammami, I., Foucher, S., Lepage, R., 2018. Flood extent mapping from time-series SAR images based on texture analysis and data fusion. Remote Sens. 10, 237.
Panteras, G., Cervone, G., 2018. Enhancing the temporal resolution of satellite-based flood extent generation using crowdsourced data for disaster monitoring. Int. J. Remote Sens. 39, 1459–1474.
Pekel, J.-F., Cottam, A., Gorelick, N., Belward, A.S., 2016. High-resolution mapping of global surface water and its long-term changes. Nature 540, 418.
Pradhan, B., Hagemann, U., Tehrany, M.S., Prechtel, N., 2014. An easy to use ArcMap based texture analysis program for extraction of flooded areas from TerraSAR-X satellite image. Comput. Geosci. 63, 34–43.
Qi, S., Brown, D.G., Tian, Q., Jiang, L., Zhao, T., Bergen, K.M., 2009. Inundation extent and flood frequency mapping using LANDSAT imagery and digital elevation models. GIScience & Remote Sens. 46, 101–127.
Rosenqvist, A., Shimada, M., Ito, N., Watanabe, M., 2007. ALOS PALSAR: a pathfinder mission for global-scale monitoring of the environment. IEEE Trans. Geosci. Remote Sens. 45, 3307–3316.
Sanders, B.F., 2007. Evaluation of on-line DEMs for flood inundation modeling. Adv. Water Resour. 30, 1831–1843.
Senthilnath, J., Shenoy, H.V., Rajendra, R., Omkar, S.N., Mani, V., Diwakar, P.G., 2013. Integration of speckle de-noising and image segmentation using Synthetic Aperture Radar image for flood extent extraction. J. Earth Syst. Sci. 122, 559–572.
Sentinel-1 Algorithms, 2019. Google Earth Engine API. Google Developers, https://developers.google.com/earth-engine/sentinel1 (accessed 6.2.19).
Sheng, Y., Gong, P., Xiao, Q., 2001. Quantitative dynamic flood monitoring with NOAA AVHRR. Int. J. Remote Sens. 22, 1709–1724.
Singha, M., Dong, J., Zhang, G., Xiao, X., 2019. High resolution paddy rice maps in cloud-prone Bangladesh and Northeast India using Sentinel-1 data. Sci. Data 6, 26.
Sulla-Menashe, D., Friedl, M.A., 2018. User guide to collection 6 MODIS land cover (MCD12Q1 and MCD12C1) product. USGS, Reston, VA, USA, pp. 1–18.
Tong, X., Luo, X., Liu, Shuguang, Xie, H., Chao, W., Liu, Shuang, Liu, Shijie, Makhinov, A.N., Makhinova, A.F., Jiang, Y., 2018. An approach for flood monitoring by the combined use of Landsat 8 optical imagery and COSMO-SkyMed radar imagery. ISPRS J. Photogramm. Remote Sens. 136, 144–153.
Torres, R., Snoeij, P., Geudtner, D., Bibby, D., Davidson, M., Attema, E., Potin, P., Rommen, B., Floury, N., Brown, M., 2012. GMES Sentinel-1 mission. Remote Sens. Environ. 120, 9–24.
Tsyganskaya, V., Martinis, S., Marzahn, P., Ludwig, R., 2018. SAR-based detection of flooded vegetation–a review of characteristics and approaches. Int. J. Remote Sens. 39, 2255–2293.
Twele, A., Cao, W., Plank, S., Martinis, S., 2016. Sentinel-1-based flood mapping: a fully automated processing chain. Int. J. Remote Sens. 37, 2990–3004.
Uddin, K., Matin, M.A., Meyer, F.J., 2019. Operational flood mapping using multi-temporal sentinel-1 SAR images: a case study from Bangladesh. Remote Sens. 11, 1581.
UNU, 2018. UNU Update: Two billion face flood danger soon. accessed 8.15.18. http://archive.unu.edu/update/archive/issue32_2.htm.
Wahlstrom, M., Guha-Sapir, D., 2015. The Human Cost of Weather-Related Disasters 1995–2015. UNISDR, Geneva, Switzerland.